J Mater Sci: Mater Med (2011) 22:1005–1014
DOI 10.1007/s10856-011-4284-9

Corrosion behaviour and biocompatibility of a novel Ni-free intermetallic coating growth on austenitic steel by hot dipping in an Al–12.6%Si alloy

M. A. Arenas · E. Frutos · L. Saldaña · A. Conde · L. Labajos-Broncano · M. L. González-Martín · J. L. González-Carrasco · N. Vilaboa

Received: 5 November 2010 / Accepted: 7 March 2011 / Published online: 25 March 2011
© Springer Science+Business Media, LLC 2011

Abstract Commercial 316 LVM austenitic stainless steel samples have been coated by immersion in a bath of molten Al–12.6%Si alloy for 120 s. The coating consists of the $Al_{12}(Fe,Cr)_3Si_2$ intermetallic. In vitro corrosion behaviour has been evaluated in the Ringer's solution by means of potentiodynamic curves and electrochemical impedance spectroscopy. The results reveal that the coated specimens exhibit lower susceptibility to localised corrosion with respect to the substrate. XPS analysis suggests that the ennoblement of the pitting potential is due to the formation of a chromium oxyhydroxide containing passive layer. The intermetallic coating shows a good biocompatibility, as demonstrated by culturing human mesenchymal stem cells isolated from bone marrow which attached, grew and differentiated to the osteoblastic lineage to a similar extent on coated and bare steels. In summary, this study proposes a method that generates Ni-free coatings of the stainless steel with useful properties for biomedical applications.

M. A. Arenas (✉) · E. Frutos · A. Conde · J. L. González-Carrasco
Centro Nacional de Investigaciones Metalúrgicas, CENIM-CSIC, Avda. Gregorio del Amo 8, 28040 Madrid, Spain
e-mail: geles@cenim.csic.es

E. Frutos · L. Saldaña · L. Labajos-Broncano · M. L. González-Martín · J. L. González-Carrasco · N. Vilaboa
Centro de Investigación Biomédica en Red de Bioingeniería, Biomateriales y Nanomedicina CIBER-BBN, Saragossa, Spain

L. Saldaña · N. Vilaboa
Hospital Universitario La Paz-IdiPAZ, Paseo de la Castellana 261, 28046 Madrid, Spain

L. Labajos-Broncano · M. L. González-Martín
Departamento de Física Aplicada, Universidad de Extremadura, Av. Elvas s/n, 06071 Badajoz, Spain

1 Introduction

The 316 Low Vacuum Melting (LVM) austenitic stainless steel is a low-cost metallic biomaterial with an easy mechanization and reasonably good biocompatibility [1, 2], widely used in the fabrication of orthopaedic devices such as bone plates, bone screws, pins, and rods. Despite its satisfactory in vitro corrosion resistance, under frictional conditions or in the presence of an aggressive medium ion release may lead to clinical complications. Metal hypersensitivity reactions are currently estimated to affect <1% of the patients with implants [3]. Ni is the most common sensitizer metal in humans, followed by Co and Cr [4, 5]. These features have triggered great activity among researchers towards the development of Ni-free steels with a large amount of nitrogen (up to 4.2 at.%) and manganese (up to 23 at.%) [6–8] or oxide dispersion strengthened (ODS) alloys [9–11]. Satisfactory results can be also obtained by the development of coatings or surface modifications. Unfortunately, most of the methods developed for Ti and their alloys are not always applicable to the steel [12].

This study deals with 316 LVM steel coated by hot dipping in an Al–Si alloy, i.e. siliconisation, which is a low-cost technique successfully used to increase the Si content at the surface without detrimental effects on the mechanical properties of the bulk. Siliconisation of 316 LVM coats the steel with a dense $Al_{12}(Fe,Cr)_3Si_2$ intermetallic coating well adhered to the substrate [13]. This coating has successfully enhanced the magnetic properties of ferritic steels [14, 15] or the oxidation resistance of Ti-aluminides [16]. Regarding the corrosion behaviour and biocompatibility of these novel intermetallic coatings, little work has been published.

From the biomedical viewpoint, the absence of Ni is pointed out as a significant advantage, whereas the high Al

content of the coating would not be a point of concern since others Al-rich aluminides, with Al contents of up to about 40 at.%, have shown good in vitro results [17, 18]. In this study, we report the in vitro corrosion behaviour and biocompatibility of 316 LVM steel modified by hot dipping in an Al–12.6%Si alloy. The electrochemical studies were performed in the Ringer's solution, to simulate the aggressiveness of the human body fluids. In vitro biocompatibility of austenitic stainless steel, before and after hot dipping, was investigated using human mesenchymal stem cells from bone marrow (hMSC), which are precursors of osteoblastic lineage.

2 Experimental procedure

2.1 Materials

Samples taken from commercial 316 LVM austenitic stainless steel bars for clinical use were supplied by the implant manufacturer (Surgival SL, Spain). This steel has the following chemical composition in wt%: Cr 17.48, Ni 14.13, Mo 2.87, Mn 1.62, Si 0.53, C 0.024, Cu 0.067, N 0.061, S 0.001, and Fe in balance.

Samples were coated by immersion of the bare alloy for 120 s in a crucible containing a melted Al–12.6%Si eutectic alloy at 765°C. After immersion, the samples were left to cool down out of the crucible. All samples become covered by an outer layer of Al–Si, remnant of the melted alloy [16]. This layer was removed by chemical etching and further mechanical abrasion with SiC papers. A final mechanical polishing to a mirror-like finishing was performed by using diamond paste and a final step with colloidal silica. After polishing, the specimens were washed in running water, sonicated in ethanol, and dried in a jet of warm air. Uncoated samples were polished using the same method.

2.2 Microstructural and surface examination

Microstructural characterization was conducted by optical and scanning electron microscopy (SEM). A JEOL JSM 6500 high resolution field emission, equipped with energy dispersive X-ray analysis (EDX), was used. Examination of the samples was made on polished cross-sections, without making any chemical etching.

X-ray photoelectron spectroscopy (XPS) analysis of the coated samples before and after exposure to the aggressive solution was performed with a K-Alpha Thermo Scientific equipment. A monochromatic Al-Kα radiation ($h\nu = 1486.92$ eV) was used. Photoelectrons were collected from a take off angle of 90° relative to the sample surface. The measurement was done in a Constant Analyser Energy mode (CAE) with a 100 and 149.7 eV pass energies for survey and individual snapshot spectra, respectively.

An elliptical X-ray spot was used with a spot diameter of 400 μm. Argon sputtering, performed in the high current mode at 3000 eV during 25 s, was carried out on the sample in order to remove impurities from its top layer. In any case, charge compensation was not needed because of the conductive nature of the sample. Binding energies were calibrated by setting the C1s hydrocarbon peak to 284.6 eV. Data acquisition and processing were done by employing Advantage software from Thermo Scientific.

2.3 In vitro corrosion behaviour

Electrochemical corrosion behaviour of the coated and uncoated stainless steel was evaluated by potentiodynamic polarization and electrochemical impedance spectroscopy (EIS) in the Ringer's solution at 37°C. This solution was chosen according to the ISO 16428:2005 (E) standard [19]. Electrochemical tests were performed using a conventional three-electrode cell. A saturated calomel electrode (SCE) was used as reference electrode, with 0.5 cm^2 of the sample to be measured as the working electrode and a platinum wire as the counter electrode. The electrodes were connected to a Gamry Instruments CMS 105 potentiostat.

The sample was held at open circuit potential for 15 min and then cathodically polarized 300 mV bellow the corrosion potential. The anodic sweep stars at this potential and proceeds at an scan rate of 0.16 mV/s, until a potential which current density reaches 0.25 mA/cm^2. Additionally, potentiodynamic curves were also recorded after 1 week of immersion.

Impedance measurements were carried out to study the evolution of the coated and uncoated specimens with immersion time in the Ringer's solution, up to 1 week. A sinusoidal potential signal of 3.53 mV (rms) was applied, with a frequency range from 100 kHz down to 10 mHz. The open circuit potential of the specimens was allowed to stabilise before the test. The results were analysed using the Equivcrt fitting program [20].

All electrochemical tests were performed at least three times for each specimen in order to ensure the reproducibility of the results.

2.4 In vitro biocompatibility assays

Purified hMSCs ($CD105^+$, $CD29^+$, $CD44^+$, $CD14^-$, $CD34^-$, $CD45^-$) were purchased from Cambrex Bio Science (Verviers, Belgium) and expanded in a defined medium (Cambrex Bio Science). Cells were maintained at 37°C under 5% CO_2 and 95% air in a humidified incubator. For cell culture experiments, 20 mm diameter discs of 316

LVM stainless steel before or after hot dipping in an Al–12.6%Si alloy were used. All the samples were routinely sterilized under UV light in a laminar flow hood for 12 h on each side and stored until use.

For cell spreading assays, cells were seeded on uncoated or coated samples in 12-well plates (1.5×10^4 cells/well) and cultured in growth medium for 1 day. Cell morphology was observed after fixation of cells with a solution of 2.5% glutaraldehyde in PBS using a spectral confocal microscope (LEICA TCS SPE, Leica microsystems, Heidelberg, GMBH, Germany). In order to quantify cell spreading, a total of 30 cells randomly selected from five representative images per sample were manually outlined, and cell areas were measured using ImageJ v1.34 image analysis software. Cell proliferation was evaluated at 1, 4 and 7 days using the alamarBlue assay (Biosource, Nivelles, Belgium), as previously described [21]. To study the assembly of fibronectin matrix, cells cultured for 1–7 days were fixed, permeabilised and stained for fibronectin (FN) and actin filaments, following the procedures described elsewhere [22]. Samples were examined using a spectral confocal microscopy.

In order to determine alkaline phosphatase (ALP), cells were seeded on uncoated or coated samples in 12-well plates (1.1×10^4 cells/well) and incubated for 7 days in osteogenic induction medium containing dexamethasone, ascorbate and β-glycerophosphate (Cambrex Bio Science). hMSC cultured in growth medium were used as controls. ALP activity was assessed in cell layers by determining the release of *p*-nitrophenol from *p*-nitrophenylphosphate and normalized to the total amount of proteins present in the lysates, following the procedures reported elsewhere [23].

The data are presented as means ± SD of three independent experiments. The differences between uncoated and coated samples were evaluated by an analysis of variance statistical method. The *P*-values < 0.05 were considered statistically significant.

3 Results and discussion

3.1 Microstructural characterization

Hot dipping of the austenitic stainless steel in a bath of molten Al–12.6%Si alloy for 120 s develops a two-layered coating, as can be seen in Fig. 1. Elimination of the outermost layer, remnant of the Al–Si melted alloy, leaves a uniform and adherent coating (see inset of Fig. 1) with a submicron grain size [13]. It is worth noting the absence of cracks or signs of delamination in the coating. Microanalysis of the cross section revealed a constant content of main elements throughout the thickness (Fig. 2). It is interesting to note the absence of compositional gradients beneath the substrate/coating interface despite the incorporation of Fe and Cr into the coating. This seems to be consistent with a gradual approach to the equilibrium composition near the coating/substrate interface corresponding to a reduction of the coating growth rate, associated with the presence of Si [24], since this element acts as an agent limiting the diffusion of Fe and Cr, due mainly to the high electron affinity that presents the Si to the Fe. The homogeneity of the chemical composition throughout the coating, Fig. 2, as well as the low contrast of the backscattered electron images (not shown) suggests the formation of a monophasic layer with an stequiometric composition, which was identified as an $Al_{12}(Fe,Cr)_3Si_2$ intermetallic compound with an hexagonal structure [13]. The absence of Ni in the coating, which is relevant for the intended application, is explained by both the absence of dilution of the substrate during hot dipping and the intermetallic nature of the forming layer, being thermodynamic that governs the type of intermetallic and the range of solubility. A detailed study of the nanomechanical properties of the coating has been presented elsewhere [25].

3.2 In vitro corrosion tests

Electrochemical behavior was evaluated to determine the corrosion resistance of the coated and uncoated steel in terms of corrosion kinetics and localized corrosion susceptibility.

Potentiodynamic polarisation curves of the bare and coated steel after 15 min of immersion in the Ringer's solution are shown in Fig. 3. Both materials exhibit a vertical anodic branch. This fact points out that either the $Al_{12}(Fe,Cr)_3Si_2$ coating or the stainless steel reveal a passive behaviour under the test conditions, although there are some differences between them.

In such passive systems, corrosion activity is determined by the passive current density depicted in the anodic passive branch. In the present case, the $Al_{12}(Fe,Cr)_3Si_2$ coating and the stainless steel reveal similar values, about 1.03×10^{-7} A/cm^2. However, susceptibility to localised attack can be also determined by the length of the passive branch. In this regard, coated and bare specimens reveal different localised corrosion resistance. Stainless steel exhibits nobler corrosion potential than the $Al_{12}(Fe,Cr)_3Si_2$ coating, −216 and −425 mV/SCE, respectively. At the same time, pitting potential, E_{pit}, ranges about −155 mV/SCE for the coated sample. This value is much lower than the one for the uncoated specimens, 693 mV/SCE. Therefore, the length of the passive stage corresponding to the coated steel is shorter than the stainless steel, 580 versus 909 mV respectively. Consequently, although both materials exhibit similar passive current density, thus similar corrosion rate, the coated specimens show higher susceptibility to localised corrosion with respect to the substrate after short immersion times, 15 min.

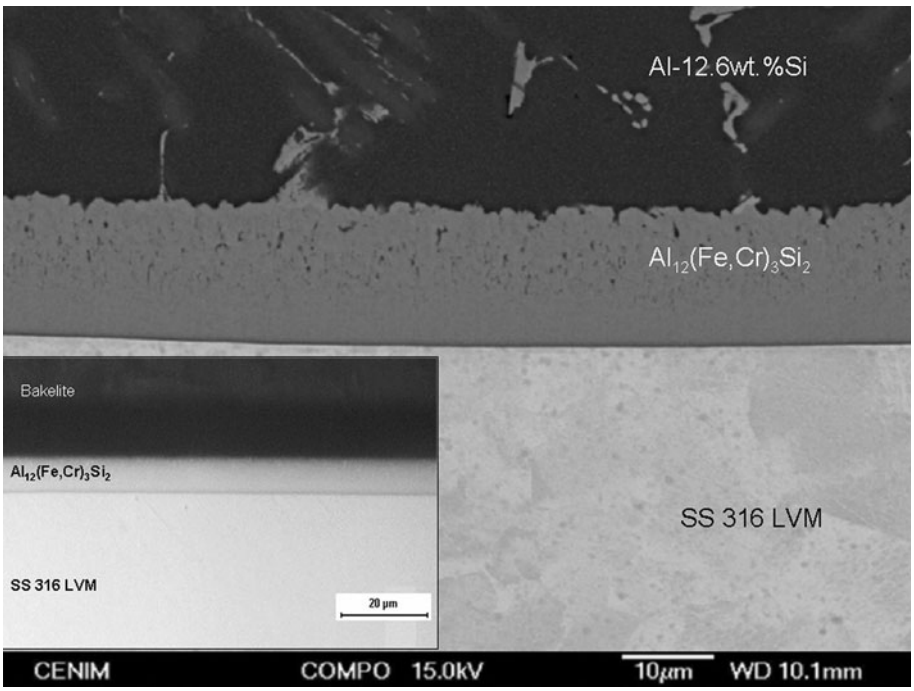

Fig. 1 Backscattered electron image corresponding to a representative cross sectional view of the sample hot dipped for 120 s. The *inset* shows an optical micrograph of the coated sample after elimination of the outermost layer

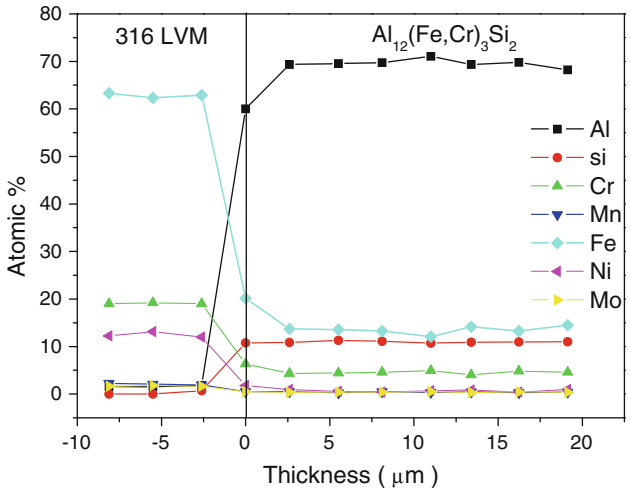

Fig. 2 Profile analysis through the coating for a sample hot dipped during 120 s

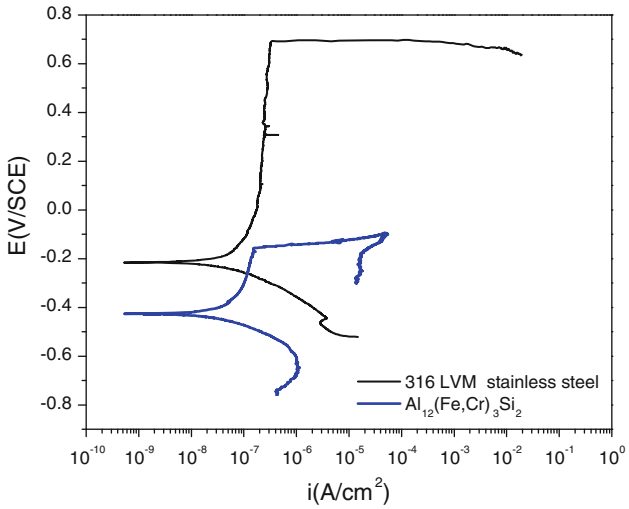

Fig. 3 Polarization curves of coated and uncoated stainless steel after 15 min in the Ringer's solution at 37°C

Conversely, after 1 week of immersion in the Ringer's solution, the curves show active–passive behaviour for both systems, Fig. 4. The anodic branch shows a rise of the current density in a potential sweep of 600 mV over the corrosion potential. After this active stage, both specimens plot a vertical branch until the pitting potential is reached. The shape of the curve is related to the growth of an oxide layer during the active stage which barrier properties lead to a passive behaviour under more oxidising conditions. Moreover, the corrosion potential of the coated steel shifts towards more cathodic values, −754 mV/SCE, with respect to shorter immersion times. On the contrary, the E_{corr} for the stainless steel increases to nobler values −152 mV/SCE, regarding the E_{corr} gathered after 15 min in solution.

For both materials the i_{corr} was estimated from Tafel slopes. Similar values, 7.4×10^{-9} and 3.2×10^{-9} A/cm^2 were obtained for coated and uncoated specimens, respectively. These values are two orders of magnitude lower than i_{corr} obtained for shorter immersion times, 1×10^{-7} A/cm^2. This means that with time there is a decrease of the electrochemical activity likely due to the coarsening of the protective oxide occurred during the immersion in Ringers' solution for 1 week.

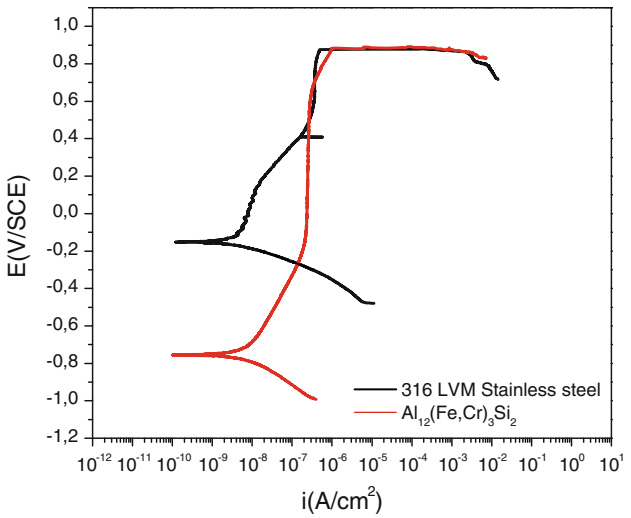

Fig. 4 Polarization curves of coated and uncoated samples, after 1 week in the Ringer's solution at 37°C

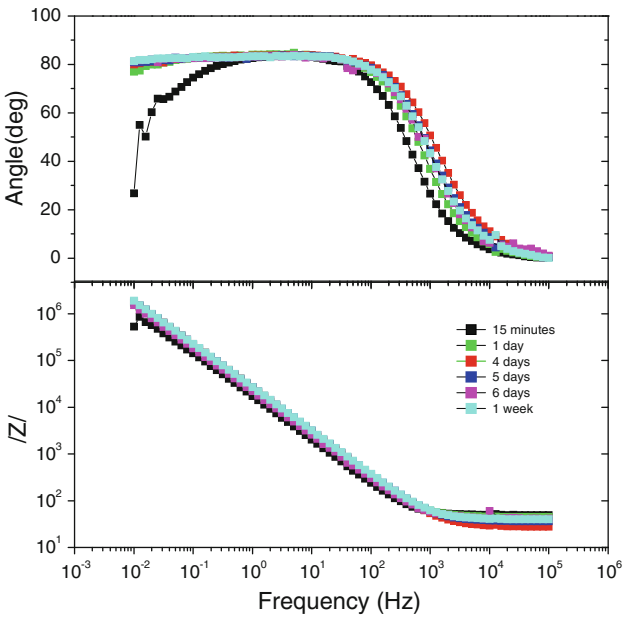

Fig. 5 Impedance spectra corresponding to uncoated samples in Ringer's solution at 37°C

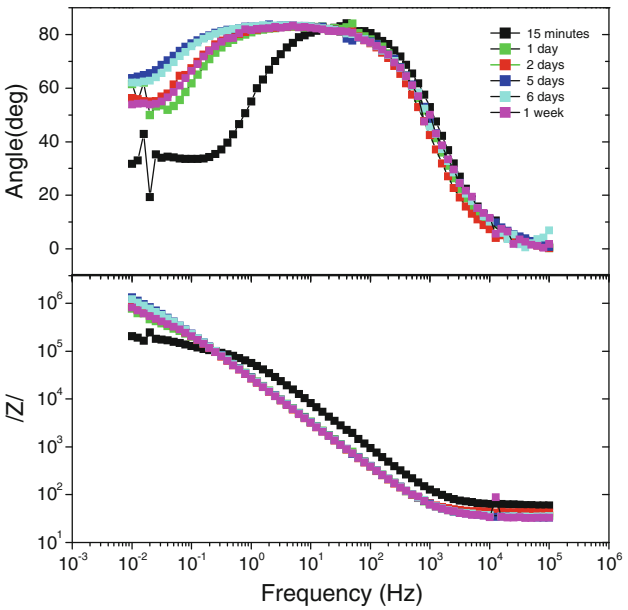

Fig. 6 Evolution of impedance spectra of $Al_{12}(Fe,Cr)_3Si_2$ coating with time in Ringer's solution at 37°C

Furthermore, the pitting potential shifts towards nobler values. This change is more significant for the coated specimen, which E_{pit} shifts about 1 V with respect to the value described for 15 min. After 1 week of immersion the E_{pit} is similar to the bare steel, 876 mV/SE, showing a notably improvement of localised corrosion susceptibility.

The stability of the $Al_{12}(Fe,Cr)_3Si_2$ coatings in the Ringer's solution was also studied by means of electrochemical impedance spectroscopy. The evolution of the impedance spectra for coated and uncoated samples is gathered in Figs. 5 and 6. Bode phase angle plot of stainless steel exhibits one time constant for all immersion times. The phase angle is about −85° for nearly all the frequency range. By using the equations described elsewhere [26] the capacitance value is about 8.6 μF/cm^2. Conversely, for $Al_{12}(Fe,Cr)_3Si_2$ coating, the Bode phase diagram after 15 min of exposure reveals two time constants. The first one is depicted as a maximum at medium–high frequencies, −85° approximately, and the capacitance value is 1.5 μF/cm^2. The second time constant appears at low frequencies as the onset of a maximum. As the immersion time increases, the maximum placed at medium–high frequencies becomes wider, while the low frequency contribution disappears. The evolution of the impedance for both specimens leads to a capacitance value ranging about 5.5 μF/cm^2 after this immersion. Such capacitance values are typical for metal/oxide double layers. Simultaneously, the modulus of the impedance Bode diagrams also show differences for both type of specimens. Stainless steel just depicts a slope close to −0.94, at medium–low frequencies. On the contrary, for the coated specimens the two contributions observed in the phase angle plots are also distinguished by two linear stages of different slopes. At medium–high frequencies the slope is about −0.92, but from 1 Hz the slope decreases significantly suggesting the presence of a diffusional response. The evolution of /Z/ Bode plot with time shows that the low frequency response disappears leading to a nearly pure capacitive behaviour.

This behaviour could be simulated using an equivalent circuit comprised of a resistor connected in series with a capacitor. However, this equivalent circuit would plot ideally a constant value for the phase angle of 90° and a slope of −1 for the whole frequency range in the /Z/ Bode

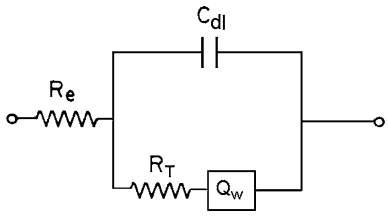

Fig. 7 Equivalent circuit used to fit the short time impedance response of the coated samples. Q_w is related to the diffusion process at low frequency

plot. In the present case, Bode diagrams show slight deviations of these ideal values, Figs. 5 and 6, so different equivalent circuit were used to model the electrochemical response obtained for each case.

Constant phase elements (CPE) instead of simple capacitors, C, [CPE = 1/C (jw) n] were used to fit the spectra. n is the frequency dispersion factor and varies from 0 to 1 and when n = 1, C can be considered as real capacitance. For the uncoated specimens, the model circuit used corresponds to a Randles equivalent circuit, while for the coated samples another electrical element needs to be incorporated in the equivalent circuit to fit the diffusional response at short times of immersion, Fig. 7. Although the relative error of the charge transfer resistance, modelled R_t, will be quite high, at least the value provides a rough idea about the corrosion resistance of both type of specimens. Table 1 shows the values of solution resistance, R_s, charge transfer resistance, R_t, the constant phase element of the double layer, C_{dl} (n), and CPE of the diffusion process, Q_w (n) at 15 min and 1 week of immersion. Simulations by means of these two equivalent circuits provide good agreement with the experimental data with Chi-squared of about 5×10^{-3}. As it can be seen, capacitance values, CPE, are similar for coated and uncoated specimens, tenths $\mu F/cm^2$, which are typical of double layer of metals. The evolution of the impedance and the capacitance values suggest that the electrochemical response is controlled by changes of the passive film on each case. So it is reasonable to relate the time constant of the system to a charge transfer process taking place in the surface covered by an oxide/hydroxide layer. In this sense, the presence of chromium in the coating might help to form a passive oxide layer with better corrosion resistance. The influence of Cr on the passive behavior on aluminum and steels has been reported previously. Rangel et al. [27] studied the influence of Cr ion implantation on Al, pointing out that certain Cr doses lead to important improvements in pitting corrosion and corrosion kinetics. Such improvements rely on the presence of Cr_2O_3 layer.

3.3 XPS analysis

Changes in the chemistry of the passive film, occurred during the immersion of the coated specimens in Ringers' solution, were studied by XPS. By comparison of the XPS spectra before and after immersion, a higher contribution of the oxidised compounds is easily observed by means of a widening and intensity increase of the oxygen peak. Survey XPS spectra was obtained after sometime of sputtering with Ar to remove surface contamination, so the peaks corresponding to the main elements—Al, Si, Fe, Cr, and O—were clearly identified.

The Cr $2p^{3/2}$ peak corresponding to a non-immersed specimen plots only one component placed at 573.8 eV, Fig. 8a. This binding energy corresponds to metallic Cr which reference value is described at 574.37 eV. However, after 1 week in the solution, this peak decomposes into two components of different intensities placed at 575.84 and 577.28 eV. These peaks are related to Cr_2O_3 (which B.E. is usually described at 575.9–576.0 eV) and $Cr(OH)_3$/CrOOH (literature B.E. for 577.3 eV).

Similarly, for the non soaked specimens, the high resolution window for Al, Si and Fe shows a high contribution of the metallic elements regarding the oxidised compounds which appear like a small shoulder at higher binding energies. The metallic components for these elements are placed at 72.13 eV for Al; 98.68 eV for Si; and 706.12 eV for Fe, Fig. 8b–d, while the oxidised components are described at 73.79, 100.2 and 707.29 eV, respectively. For comparison purposes, Table 2 gathers the theoretical and experimental B.E. for each element and the corresponding compounds.

Conversely, after 1 week in the solution, the peaks related to oxidised compounds undergo an increase of intensity becoming more relevant to the metallic component, which notably decreases for these three elements. The highest component of Al 2p placed at 74.27 eV becomes wider. This peak could be related to aluminium hydroxides—AlO(OH), $Al(OH)_3$—which according to literature might appear at energies between 73 and 77 eV. These changes are even more pronounced for the Si 2p, which metallic contribution placed at 98.10 eV appears clearly separated from the oxide peak at 101.36 eV. This energy corresponds to Si^{2+} (referenced at 101.3 eV). Finally, the Fe 2p peak can be fitted with two components at 708.5 and 709.93 eV. These can be attributed to an oxide type Fe_3O_4 (referenced at 708.2 eV), and Fe_2O_3 with a referenced energy of 710.8 eV [28, 29]. These findings are supported by the evolution of the O 1s peak, Fig. 8e, which can be fitted by three components. Two of them are located at 529.43 and 530.19 eV, which would correspond to Fe_2O_3 and Fe_3O_4, but also with Cr^{3+}, Si^{2+} and Al oxides. Finally, the last peak, placed at 531.31 eV would be related to chromium hydroxide—$Cr(OH)_3$.

The XPS results corroborate the electrochemical behaviour in the Ringers' solution. The presence of a Cr^{3+} state corresponding to the chromium oxyhydroxide phase

Table 1 Values of corrosion parameters obtained from impedance spectra at 15 min and 1 week of immersion

	R_s (Ω cm^2)	R_t (Ω cm^2)	C_{dl} (μF/cm^2)	n	Q_w (μF/cm^2)	n
15 min						
Coated specimens	62.07	8.97×10^4	2.39	0.95	21.60	0.49
Stainless steel	49.52	1.22×10^6	10.50	0.93	–	–
1 week						
Coated specimens	34.56	3.62×10^6	6.93	0.91	–	–
Stainless steel	37.07	2.69×10^7	6.87	0.93	–	–

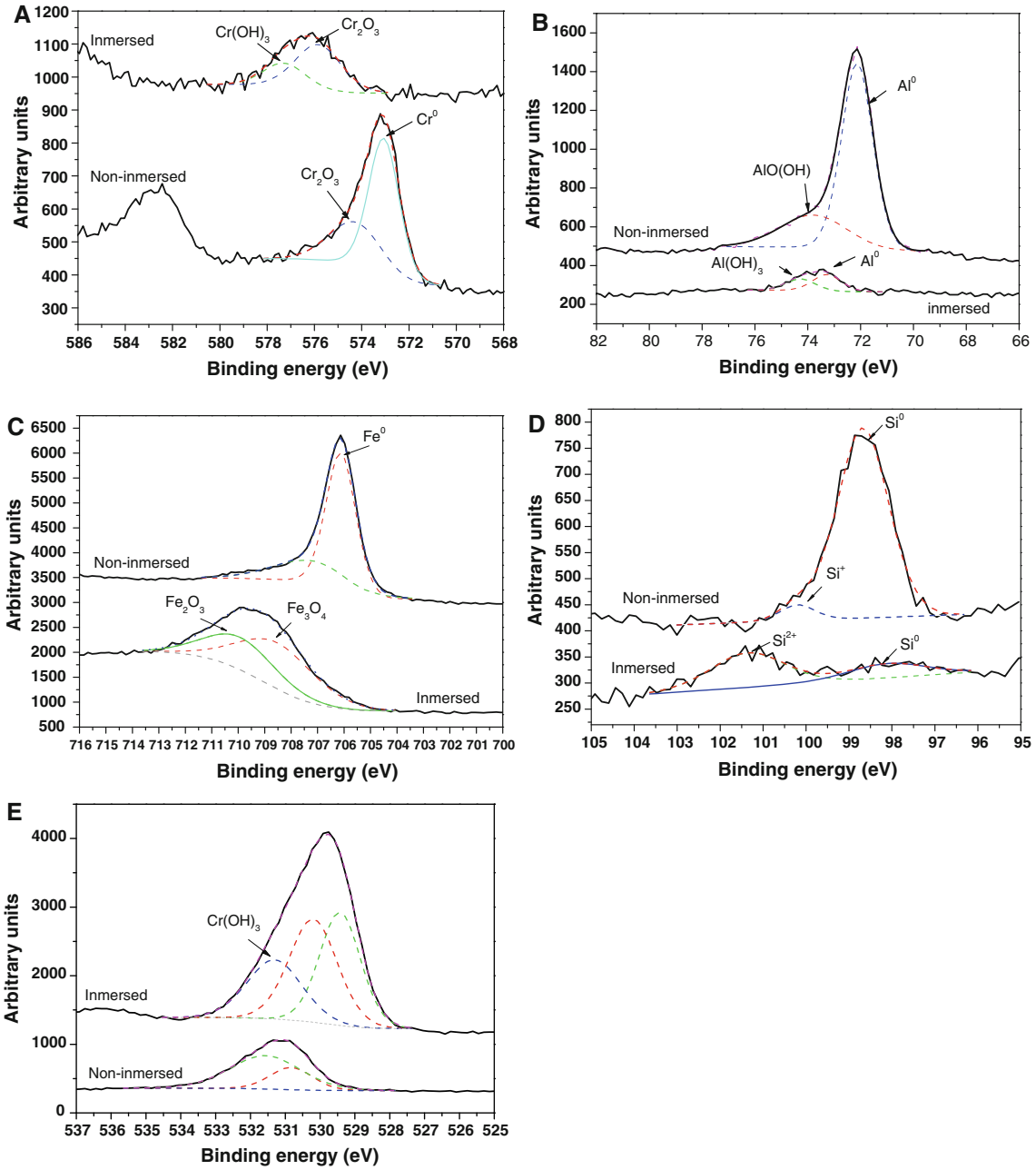

Fig. 8 XPS spectra for coated specimens before and after the exposure in Ringers' solution for **a** Cr 2p$^{3/2}$, **b** Al 2p, **c** Fe 2p, **d** Si 2p and **e** O1s

Table 2 Experimental and theoretical binding energies for Al, Cr, Fe and Si

No immersion	1 week	State	Theoretical
72.13	73.27	Al^0	73 ($2p^{3/2}$)
73.79	–	AlO(OH)	74.20
–	74.27	$Al(OH)_3$	74.30
–	–	Al_2O_3	75.7
573.8	–	Cr^0	574.37
–	575.84	Cr_2O_3	575.9–576.0
–	577.28	$Cr(OH)_3$	577.30
706.12	–	Fe^0	706.6
–	708.51	Fe_3O_4	708.2
–	709.93	Fe_2O_3	709.8
98.68	98.1	Si^0	99.2 ($2p^{3/2}$)
–	–	Si^0	99.8 ($2p^{1/2}$)
100.2	–	Si^+	100.5
–	101.36	Si^{2+}	101.3
–	–	Si^{3+}	102.3
–	–	Si^{4+}	103.4 (2p)

might be the responsible for the ennoblement of the pitting potential of the coated specimens after 1 week of immersion.

3.4 Cell culture assays

Changes in surface chemistry of stainless steel surfaces may affect the biocompatibility of the alloy [30–33]. As siliconisation of 316 LVM developed an $Al_{12}(Fe,Cr)_3Si_2$ intermetallic coating, we examined hMSCs responses to the surface, in terms of adhesion, viability and maturation. Fluorescence images revealed that cells cultured on both uncoated and coated samples exhibit classical aspects of slightly elongated polygonal spreading, Fig. 9a. As expected, the quantified areas of cells cultured on the intermetallic coatings were similar to those measured on bare steel. Measurement of metabolic activity was used to monitor cellular viability. The number of viable cells increased for 1–7 days to a similar extent on both uncoated and hot dipped samples, Fig. 9b. Microscopic examination of cells cultured for 1–7 days on the samples displayed actin filaments organized in well-defined stress fibres and mostly oriented in a parallel direction following the main cellular axis, Fig. 10a. Actin network organization was unaffected by the coating. FN is a noncollagenous matrix component secreted by cells as a soluble dimer, which assembles at the cell surface into an insoluble dense meshwork of interconnected fibrils [34]. FN fibrils formed an extensive network that could be observed between the cells as well as across the cell surface, and paralleled the alignment of the actin filaments, Fig. 10a. Matrix fibronectin deposition increased for the entire culture time. No differences in cellular distribution of FN were found between uncoated and coated samples. In order to evaluate the ability of the intermetallic coating to promote osteogenic maturation, hMSCs were switched to the osteoblastic phenotype by incubation in media containing specific inducers of cell differentiation. We observed that the activity of ALP, a marker of the osteoblastic phenotype, increased to a same extent on hot dipped samples than on bare steel, Fig. 10b. In summary, cell culture experiments indicate that the intermetallic coating obtained by means of hot dipping allows cell adhesion and proliferation, the assembly of an extracellular matrix and the maturation of functional bone-forming cells, demonstrating its potential to be used in the fabrication of orthopaedic devices.

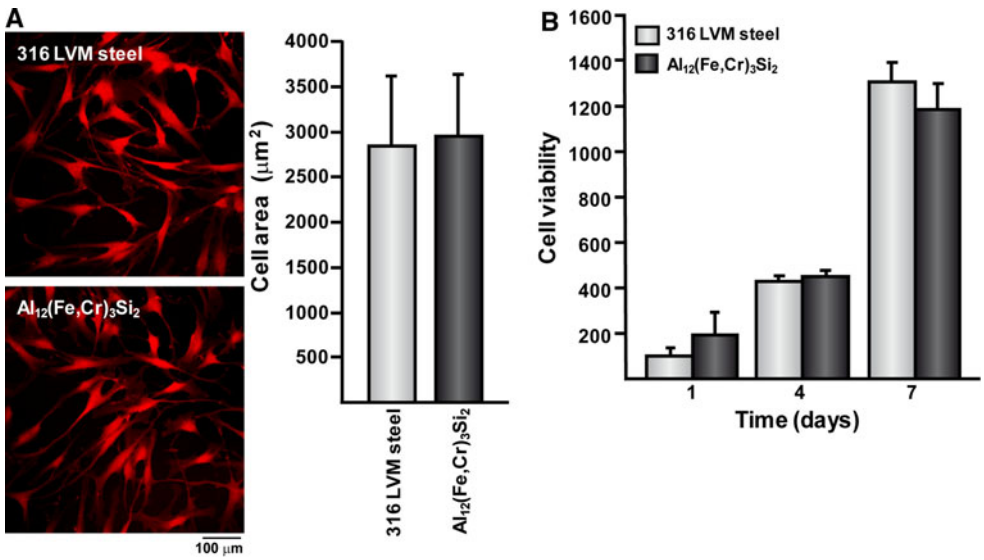

Fig. 9 **a** Confocal maximum projections showing glutaraldehyde fixed cells (*red*) on the samples. The graph shows the cell area measurements. **b** Cell proliferation on coated and uncoated samples. The data are expressed as percentages of the fluorescence measured on cells cultured on uncoated samples for 1 day, which were given the arbitrary value of 100

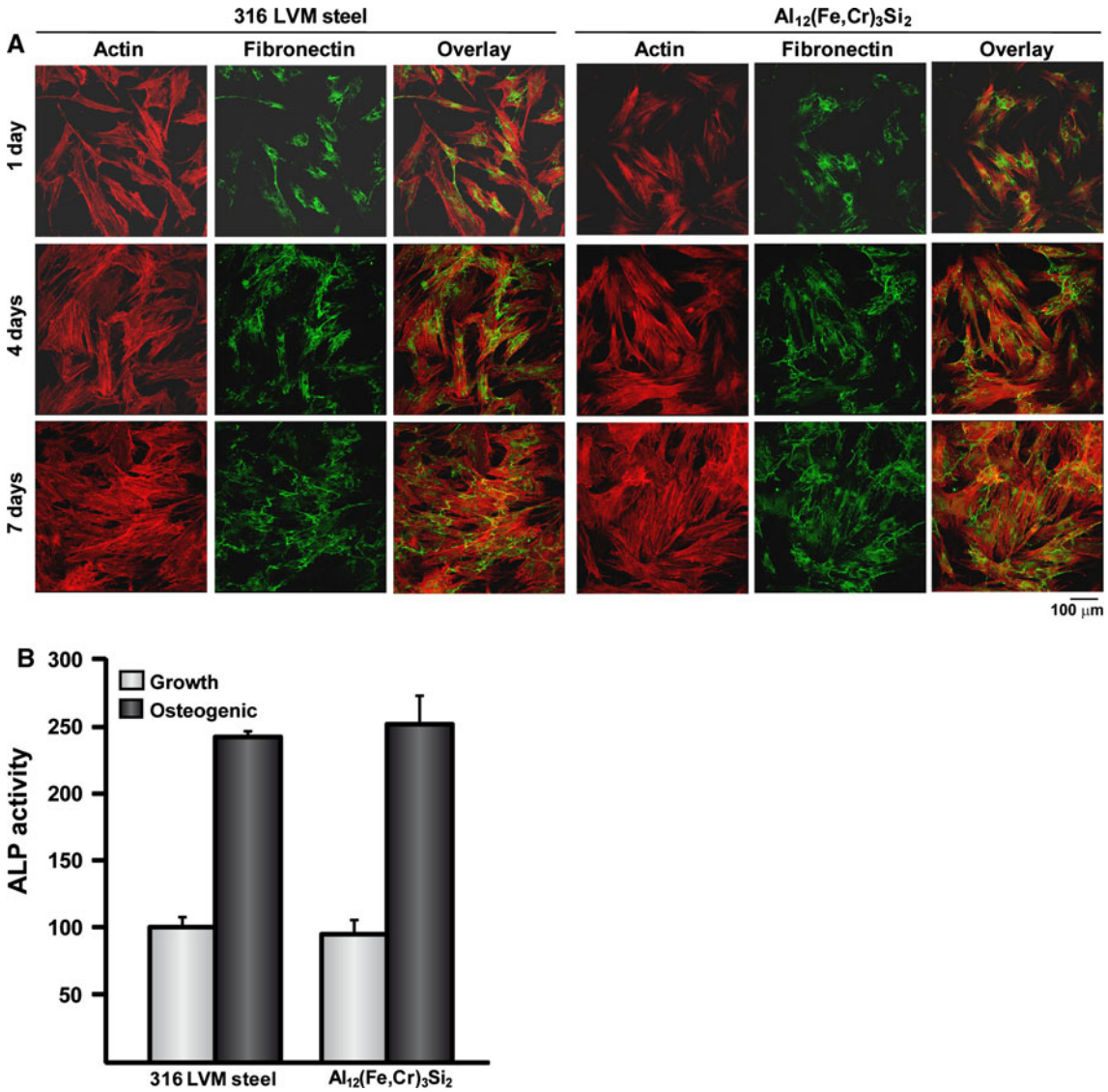

Fig. 10 **a** Confocal maximum projections showing cells stained for actin and FN on the samples. **b** ALP activity on coated and uncoated samples. The data are expressed as percentage of the absorbance measured on cells cultured on uncoated samples in growth medium, which was given the arbitrary value of 100

4 Conclusions

The generation of coatings on stainless steel 316 LVM through siliconisation in liquid phase seems to be a promising method to obtained intermetallic coatings for biomedical applications. The corrosion tests conducted in Ringer's solution show that after 1 week of immersion, intermetallic compound reveals a similar corrosion rate to that of stainless steel, while the resistance to localized attack is greater. The enhancement of the protective properties is due to the presence of Cr in the coatings which develops a chromium oxide layer as result of the immersion in Ringer's solution. The coating may be a promising alternative for the fabrication of orthopaedic implants since it does not compromise the good in vitro biocompatibility of the stainless steel.

Acknowledgments This work was supported by grants MAT2006-12948-C04-01-02-03 and MAT2009-14695-C04-C01-02-03 from the Ministerio de Ciencia e Innovación (Spain), and grants from Fundación Mutua Madrileña. N.V. is supported by program I3SNS from Fondo de Investigaciones Sanitarias (Spain). We thank Fatima Bensiamar (CIBER-BBN, Spain) for excellent technical support.

References

1. Schmidt C, Ignatius AA, Claes LE. Proliferation and differentiation parameters of human osteoblasts on titanium and steel surfaces. J Biomed Mater Res. 2001;54:209–15.

2. Anselme K, Noël B, Hardouin P. Human osteoblast adhesion on titanium alloy, stainless steel, glass and plastic substrates with same surface topography. J Mater Sci Mater Med. 1999;10:815–9.
3. Merritt K, Rodrigo JJ. Immune response to synthetic materials. Sensitization of patients receiving orthopaedic implants. Clin Orthop Relat Res. 1996;326:71–9.
4. Basketter DA, Briatico-Vangosa G, Kaestner W, Lally C, Bontinck C, Nickel WJ. Cobalt and chromium in consumer products: a role in allergenic contact dermatitis? Contact Dermatitis. 1993;28:15–25.
5. Yamamoto A, Kohyama Y, Hanawa T. Mutagenicity evaluation of forty-one metal salts by the umu test. J Biomed Mater Res. 2002;59:176–83.
6. Menzel J, Kirschner W, Stein G. High nitrogen containing Ni-free austenitic steels for medical applications. ISIJ Int. 1996;36:893–900.
7. Yamamoto A, Kohyama Y, Kuroda D, Hanawa T. Cytocompatibility evaluation of Ni-free stainless steel manufactured by nitrogen adsorption treatment. Mater Sci Eng C. 2004;24:737–43.
8. Fini M, Aldini N, Torricelli P, Giavaresi G, Borsari V, Lenger H, Bernauer J, Giardino R, Chiesa R, Cigada A. A new austenitic stainless steel with negligible nickel content: an in vitro and in vivo comparative investigation. Biomaterials. 2003;24:4929–39.
9. González-Carrasco JL, Ciapetti G, Montealegre MA, Pagani S, Chao J, Baldini N. Evaluation of mechanical properties and biological response of an alumina forming Ni-free ferritic alloy. Biomaterials. 2005;26:3861–71.
10. Strehl G, González-Carrasco JL, Peris JL, Montealegre MA, García S, Atienza C, Borchardt G. Application of thermal oxidation in the development of PM 2000 as potential biomaterial for medical devices. Surf Coat Technol. 2006;201:148–56.
11. Ciapetti G, González-Carrasco JL, Savarino L, Montealegre MA, Pagani S, Baldini N. Quantitative assessment of the response of osteoblast- and macrophage-like cells to Ni-free Fe-base alloy particles. Biomaterials. 2005;26:849–59.
12. Liu X, Chu PK, Ding C. Surface modification of titanium, titanium alloys, and related materials for biomedical applications. Mater Sci Eng R. 2004;47:49–121.
13. Frutos E, González-Carrasco JL, Capdevila C, Jiménez JA, Houbaert Y. Development of hard intermetallic coatings on austenitic stainless steel by hot dipping in an Al-Si alloy. Surf Coat Technol. 2009;203:2916–20.
14. Ros-yañez T, Houbaert Y. High-silicon steel produced by hot dipping and diffusion annealing. J Appl Phys. 2002;91:7857–9.
15. Ros-Yañez T, Houbaert Y, Schneeweiss O, Asensio J, Prado M. Acero de alto silicio producido por inmersión en Al-Si y recocido de difusión. Rev Metal Madrid. 2000;36:339–47.
16. Xiong HP, Mao W, Ma WL, Xie YH, Feng Y, Yuan H, Li XH. Liquid-phase aluminizing and siliconizing at the surface of a Ti60 alloy and improvement in oxidation resistance. Mater Sci Eng A. 2006;433:108–13.
17. González-Carrasco JL, Ciapetti G, Montealegre MA, Savarino L, Muñoz-Morris MA, Baldini N. Potential of FeAlCr intermetallics reinforced with nanoparticles as new biomaterials for medical devices. J Biomed Mater Res B Appl Biomater. 2007;80:201–10.
18. Denizard OR, Carlo ND, Navas V, Sundaram PA. Biocompatibility studies of human fetal osteoblast cells cultured on gamma titanium aluminide. J Biomed Mater Res Mater Med. 2008;19:153–8.
19. ISO 16428 (E) Implants for surgery—test solutions and environmental conditions for static and dynamic corrosion tests on implantable materials and medical devices. 2005. http://www.iso.org.
20. Boukamp BA. A package for impedance/admittance data analysis. Solid State Ionics. 1986;18 & 19:136–40.
21. Saldaña L, Vilaboa N. Effects of micrometric titanium particles on osteoblast attachment and cytoskeleton architecture. Acta Biomater. 2010;6:1649–60.
22. Saldaña L, Méndez-Vilas A, Jiang L, Multigner M, González-Carrasco JL, Pérez-Prado MT, González-Martín ML, Munuera L, Vilaboa N. In vitro biocompatibility of an ultrafine grained zirconium. Biomaterials. 2007;28:4343–54.
23. Saldaña L, Sánchez-Salcedo S, Izquierdo-Barba I, Bensiamar F, Munuera L, Vallet-Regí M, Vilaboa N. Calcium phosphate-based particles influence osteogenic maturation of human mesenchymal stem cells. Acta Biomater. 2009;5:1294–305.
24. Eggeler G, Auer W, Kaesche H. On the influence of silicon on the growth of the alloy layer during hot dip aluminizing. J Mater Sci. 1986;21:3348–50.
25. Frutos E, Martínez-Morillas R, González-Carrasco JL, Vilaboa N. Nanomechanical properties of novel intermetallic coatings developed on austenitic stainless steels by siliconisation in liquid phase. Intermetallics. 2011;19:260–6.
26. Walter GW. A review of impedance plot methods used for corrosion performance analysis of painted metals. Corros Sci. 1986;26:681–703.
27. Rangel CM, Paiva TIC. Chromium ion implantation for inhibition of corrosion of aluminium. Surf Coat Technol. 1996;83:194–200.
28. Zhang YS, Zhu XM, Liu M, Che RX. Effects of anodic passivation on the constitution, stability and resistance to corrosion of passive film formed on an Fe-24Mn-4Al-5Cr alloy. Appl Surf Sci. 2004;222:01–89.
29. Phadnis SV, Satpati AK, Muthe KP, Vyas JC, Sundaresan R. Comparison of rolled and heat treated SS304 in chloride solution using electrochemical and XPS techniques. Corros Sci. 2003;45:2467–83.
30. Bordji K, Jouzeau JY, Mainard D, Payan E, Delagoutte JP, Netter P. Evaluation of the effect of three surface treatments on the biocompatibility of 316L stainless steel using human differentiated cells. Biomaterials. 1996;17:491–500.
31. Torricelli P, Fini M, Borsari V, Lenger H, Bernauer J, Tschon M, Bonazzi V, Giardino R. Biomaterials in orthopedic surgery: effects of a nickel-reduced stainless steel on in vitro proliferation and activation of human osteoblasts. Int J Artif Organs. 2003;26:952–7.
32. Hao L, Lawrence J, Phua YF, Chian KS, Lim GC, Zheng HY. Enhanced human osteoblast cell adhesion and proliferation on 316 LS stainless steel by means of CO2 laser surface treatment. J Biomed Mater Res B Appl Biomater. 2005;73:148–56.
33. Shahryari A, Omanovic S, Szpunar JA. Enhancement of biocompatibility of 316LVM stainless steel by cyclic potentiodynamic passivation. J Biomed Mater Res A. 2009;15:1049–62.
34. Baneyx G, Baugh L, Vogel V. Coexisting conformations of fibronectin in cell culture imaged using fluorescence resonance energy transfer. Proc Natl Acad Sci USA. 2001;98:14464–8.